Conformational and conductance fluctuations in a single-molecule junction: Multiscale computational study

Hu Sung Kim and Yong-Hoon Kim*

Department of Materials Science and Engineering, University of Seoul, 90 Jeonnong-dong, Dongdaemun-gu, Seoul 130-743, Korea

(Received 8 January 2010; revised manuscript received 25 June 2010; published 10 August 2010)

The key difficulty of interpreting single-molecule junction experiments arises from the uncertainties in the molecule-metal contact configurations. As an initial step toward theoretically resolving the problem, we apply a multiscale computational approach that automates force-field (FF) molecular-dynamics (MD) simulations and density-functional theory (DFT) and matrix Green's function calculations to study the correlation between the conformational and conductance fluctuations in an ideal hexanedithiolate (C6DT) single-molecule junction model. From the 300 K MD simulations of the junction model with the molecule-metal contacts modeled by the bonding of the sulfur linker atoms to the flat Au(111) surfaces, we observe noticeable movements of the S atoms that hop between hollow sites, and confirm that the potential surface derived from (Becke-3-Lee-Yang-Parr-DFT-derived) FF is fairly consistent with that obtained with (Perdew-Burke-Ernzerhof) DFT. The corresponding conductance histogram results in a single well-defined conductance peak irrespective of the C6DT mobility, so we conclude that while the multiple conductance peaks reported in several experiments cannot be explained with the considered ideal S-Au binding geometry, it can serve as a reference for more realistic molecule-metal contact models. Because the energetically preferable hollow sites correspond to the low-value side of the conductance distribution, we find that thermal fluctuations result in a slightly increased C6DT peak conductance value compared with that from the zero-temperature energy-minimized structure and that the conductance histogram can be better fit on a logarithmic scale.

DOI: 10.1103/PhysRevB.82.075412 PACS number(s): 85.65.+h, 73.63.−b, 61.46.−w, 85.35.−p

I. INTRODUCTION

With the rapid progress in nanoelectronics, it is becoming more relevant and important to develop the capacity to understand and predict the charge transport properties of nanoscale junctions on the atomistic scale. In this context, thanks to the significant experimental advances made in the last several years, single-molecular junctions provide an ideal test ground where quantitative comparisons between theory and experiment can be attempted.[1,2] Compared with previous experimental approaches, the new mechanical break junction (MBJ) experiments reported a much smaller distribution of the conductance by making it possible to form single-molecule junctions more reliably and reproducibly.[1–6] In spite of these exciting developments, there remains important qualitative as well as quantitative disagreement in the MBJ experiments. For the simple hexanedithiolate (C6DT) molecule in contact with Au electrodes $[\mathrm{Au-S(CH_2)_6S-Au}]$, whereas the distribution is significantly smaller than that in previous experiments, the reported conductance values still range from $G \approx 2.1 \times 10^{-5} G_0$ to $2.6 \times 10^{-3} G_0$ (in units of the conductance quantum $G_0 = 2e^2/h$).[1,3,7–11] Especially, multiple conductance peaks were observed, and, although they were interpreted as a manifestation of different molecule-electrode bonding geometries (and molecular structures),[7–9] their exact nature is still in dispute.[10]

Because the information on the contact atomic geometries cannot be directly extracted from experiments, atomistic computer simulations can play a crucial complementary role in clarifying the situation. However, most previous theoretical works were restricted to the zero-temperature energy-minimized structures (and thus a selected set of molecule-electrode contact configurations).[12–14] Considering that the random selection of static geometries does not objectively sample dynamically preferred junction configurations, molecular-dynamics (MD) simulations that provide rather unbiased molecular and molecule-electrode geometries are highly desirable. Such works recently began to appear,[15–18] however, only a few addressed the dynamical rearrangement of the molecule-metal contacts. In Ref. 15 Andrews *et al.* combined the classical force-field (FF) MD simulations and semiempirical Hükel-conductance calculations. On the other hand, in Ref. 16, Paulsson *et al.* employed first-principles density-functional theory (DFT) both for the MD and conductance calculations. Thus, the former approach significantly sacrificed the computational accuracy to sample a large number of contact geometries whereas the latter work explored only a limited geometrical phase space at a very high computational accuracy.

In our previous works, we developed a multiscale computational approach that combines FF MD simulations that capture the molecular *and molecule-metal contact* geometries of molecular junctions emerging from thermal fluctuations and DFT and DFT-based matrix Green's function (MGF) calculations carried out for the sampled structures that provide the junction conductance.[19–22] Compared with the two approaches described above, we believe that our scheme achieves a balanced compromise between the computational accuracy and the size of explored phase space. However, this multiscale computational procedure that involves three different software packages was relatively complicated and time consuming, which made the consideration of thermal-fluctuation effects in molecular junctions rather limited.[19] To overcome the computational bottleneck, we have recently automated our multistep processes by developing Python scripts, and here we apply them to investigate the energy and

 ©2010 The American Physical Society

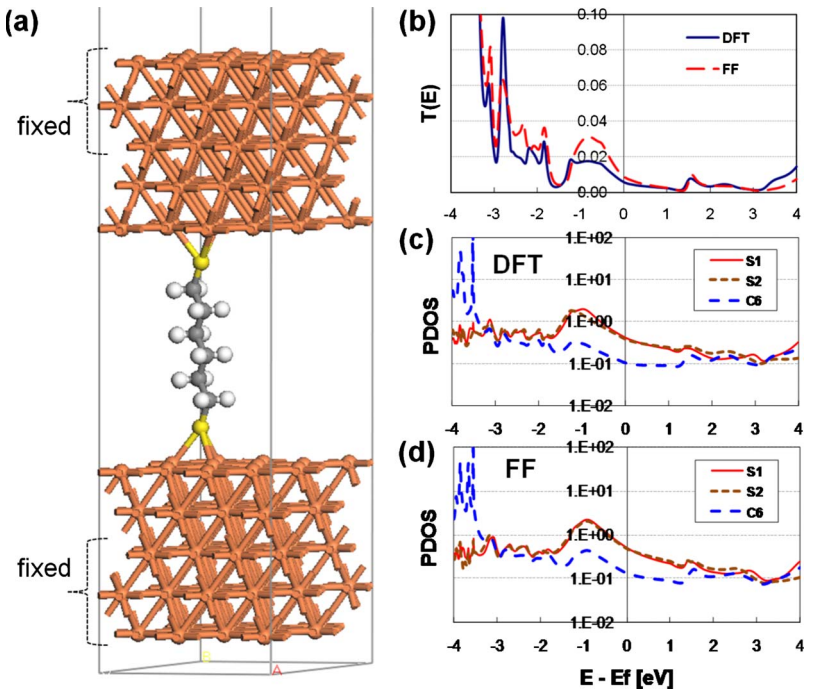

FIG. 1. (Color online) (a) The C6DT single-molecule junction model adopted in this work. The two surface-layer Au electrode atoms as well as the molecule were allowed to move. (b) The transmission curves obtained for the DFT-optimized (solid lines) and FF-optimized (long-dashed lines) geometries. The PDOS of the two S atoms (solid and short-dashed lines for the bottom and top S atoms, respectively) and the remaining molecular core (long-dashed lines) from the (c) DFT and (d) FF geometry optimizations are shown on a logarithmic scale.

conductance fluctuations accompanying thermal fluctuations of the junction. While the details of the developed multiscale scripting approach will be presented elsewhere, we will in this work focus on the accuracy of our FF in describing the thermal fluctuations of the S-Au contacts, which is presumably the key to elucidating the present experimental controversy. The adopted junction model is based on a C6DT sandwiched between flat Au(111) surfaces. The ideal metal-molecule contact geometry that does not involve Au clusters, wires, or step edges that can possibly form at the MBJ tips, might be a drastic simplification of real experimental situations but represents a well-defined reference point for the study of more realistic contact geometries. We here confirm that this contact model indeed results in a single well-defined conductance peak irrespective of the C6DT hopping on the Au surface. In addition, for the present contact model, we observe that the S-Au contact geometries of the optimized structures correspond to the low-value regime in the conductance histograms, which leads to positively skewed conductance distributions on a normal scale and a better Gaussian fitting on a logarithmic scale. This relation between the S-Au binding structures and conductance properties also results in a slightly increased MD-derived peak conductance value compared with that from the energy-minimized structures.

II. MODEL AND METHODS

The junction model we consider in this work is a C6DT molecule stretched between mirror symmetrically placed five-layer $(2\sqrt{3}\times 2\sqrt{3})R30°$ Au(111) slabs [Fig. 1(a)]. In the initial energy-minimized configuration, the electrode-electrode gap distance was 14.1 Å, and the S linker atoms were positioned at the energetically favored fcc-hollow sites of the bottom and top Au(111) surfaces. This model was derived from our earlier studies of the *N*-alkanedithiolate (N=6, 8, 10, 12, and 16) single-molecular junctions and their monolayer counterparts at the geometries optimized within DFT.[23–25] As emphasized earlier,[23,24] we regard the flat-electrode models as an idealization but they could serve as a starting point for the study of more realistic molecule-electrode contact geometries[7,9,13,16] One of the main objectives of the present work is to check the extent of validity of this hypothesis for the finite-temperature situation.

We applied to the junction model a multiscale computational approach that consists of the following three stages: (1) first, canonical-ensemble (*NVT*) classical FF MD simulations were conducted to generate atomistic MD snapshot structures. Next, for each MD snapshot, we carried out (2) quantum-mechanical DFT electronic-structure calculations, and (3) MGF coherent charge transport properties calculations. The details of our scheme were described in our previous reports (MD calculations in Refs. 20, 21, and 26 and DFT and MGF calculations in Refs. 23–26), and here we only point out the relevant points specific to this study. The first-stage MD simulations (step 1) were carried out using the above-described initial configuration within the extended Dreiding FF (Ref. 27) at the temperature of 300 K with a 1 fs time step. During the MD simulation while the outer three layers of each Au(111) slab were fixed to the original bulk positions for the accurate MGF calculations (step 3),[24] the C6DT molecule *as well as the two surface-layer* Au *atoms in each electrode* were allowed to thermally fluctuate without any constraint. After the initial 50 ps equilibration MD steps, 300 MD snapshots were sampled at the intervals of 0.5 ps for the DFT calculations (step 2). Here, the Perdew-Burke-Ernzerhof parameterization of the generalized gradient approximation (GGA),[28] norm-conserving pseudopotentials,[29] and a double-ζ-polarization-quality Gaussian basis set optimized for the corresponding GGA pseudopotentials were employed. A single $\mathbf{k}_{\parallel}$ point shifted off from the Γ point was sampled along the electrode-surface direction. For the MGF

TABLE I. The atomic geometries of the C6DT single-molecule junction model from the FF and the DFT geometry optimizations, and the root-mean-square (rms) difference between the two junction models. $Au_{L1(L2)}$ is the center-of-mass position of the first (second) surface-layer Au atoms and Au_3 is the three Au atoms closest to the S anchor atoms. The interlayer distance within the bulk Au is 2.353 Å, and the rms deviation between FF and DFT junction geometries is 0.119 Å. Tilt angle was defined as the angle between the S-S line and the Au surface-normal direction. Units are degree for the angles and angstrom for the distances.

Model	Tilt angle	Au_{L1}-Au_{L2} distance	Au_3-S distance	S-C distance	C-C distance	S-S distance	Au-Au distance
FF	0.14	2.419	2.715	1.819	1.556	9.602	14.084
DFT	0.77	2.463	2.734	1.878	1.540	9.555	13.873
Difference	−0.63	−0.044	−0.028	−0.062	0.017	0.047	0.211

calculations (step 3), we adopted the C6DT *plus the two surface layers from each* Au *electrode* as the scattering region [Fig. 1(a)]. To calculate the surface Green's functions corresponding to each electrode, we performed DFT calculations using four $k_\perp$ points along the surface-normal direction. With these parameters, we avoid the band alignment problem and obtain highly converged transmission data.[24]

We have automated steps 2 (DFT) and 3 (MGF), for which the computational input corresponding to all the MD snapshots are identical except for the atomic coordinates and thus patterns for scripts can be easily extracted. The codes were written in Python language, which is particularly suitable for gluing standalone applications,[30] and their details will be reported elsewhere. In Sec. III, we will instead consider the energetics of the C6DT junction described within FF and DFT, and next analyze the conductance $G \equiv T(E=E_F)$ histograms emerging from MD simulations. In considering the conductance data, we will limit ourselves to the low-voltage coherent tunneling limit, for which the usual adiabatic or Born-Oppenheimer approximation can be invoked and the coupling between the transporting charge and the molecular vibration is negligible.[31]

III. RESULTS AND DISCUSSIONS

A. Reference zero-temperature results

Before discussing the thermally fluctuating C6DT single-molecule junction, we first consider its energy-minimized states with the focus on the comparison of FF- and DFT-derived results. Comparison of the atomic geometries optimized within FF and DFT is summarized in Table I, the conductance data calculated for the two structures are shown in Fig. 1(b), and the corresponding projected density-of-states (PDOS) curves are presented in Figs. 1(c) and 1(d), respectively. Table I shows that our FF parameters faithfully reproduce the DFT geometries including the swelling of the Au surface atoms, with the biggest difference in the bond lengths being the S-C distance of 0.062 Å. This small geometrical difference naturally results in a minor difference in the PDOS data (Note that they are shown on a logarithmic scale) but a rather noticeable difference in the conductance values: $G=5.94\times10^{-3}G_0$ for the DFT-optimized structures and $G=9.06\times10^{-3}G_0$ for the FF-optimized structure, respectively. This indicates the order of errors that can be expected in the FF-derived conductance data presented below and suggests that they are slight overestimates of the purely GGA-based results. However, such quantitative differences are insignificant compared to the experimental and computational indeterminacies and should not affect our conclusions qualitatively. The quality of our FF parameters will be further discussed in Sec. III B.

Finally, we point out that, as discussed previously,[23–25] the nature of the charge transport channels can be analyzed in terms of the PDOS data [Figs. 1(c) and 1(d)]. They show that the alkane molecular cores effectively behave as an insulating barrier due to the very large energy gaps between their highest occupied molecular orbital (HOMO) and lowest unoccupied molecular orbital (LUMO) levels. The conductance of alkanedithiolates is dominated by the S linker atoms whose levels are located around $E_F-1.0$ eV, which implies that the conductance fluctuations of the C6DT will be mainly determined by the structural fluctuations of molecule-electrode contacts.[23–25]

B. Finite-temperature results

We now consider the C6DT single-molecule junction fluctuating at a finite temperature 300 K. In Fig. 2(a), we show the MD trajectories of the bottom S atom of C6DT and the first surface-layer Au atoms of the bottom electrode, which were also allowed to fluctuate in the MD simulations as shown in Fig. 3(a). At 300 K, the C6DT molecule shows a clear mobility on the Au(111) surface, in agreement with experimental observations.[32] For comparison, at a reduced temperature of 200 K, the S atoms were found to stay at the initial fcc-hollow sites throughout the MD simulations. The mobile S atom spends most of the time at the global-minimum fcc-hollow site. The bottom S atom also temporarily visits neighboring local-minimum hcp-hollow sites but, because of the constraint imposed by the top S atom that is still located at the fcc-hollow site of the top Au(111) surface, it hops back to the original fcc-hollow site. Whereas the bridge sites are briefly visited during the back-and-forth hopping between the fcc and two neighboring hcp sites, the energetically unfavorable on-top sites are not visited. The top S atom shows an overall similar trajectory, which results in the minimum, maximum, and average tilt angle of C6DT with respect to the Au(111) surface-normal direction as 0.46°, 10.84°, and 3.21°, respectively. The center-of-mass distance between the top and bottom Au surface layers, the distance between the top and bottom S atoms, and the average distances between S atoms and the nearest three Au atoms at the minimum C6DT tilt angle (0.46°) configuration were

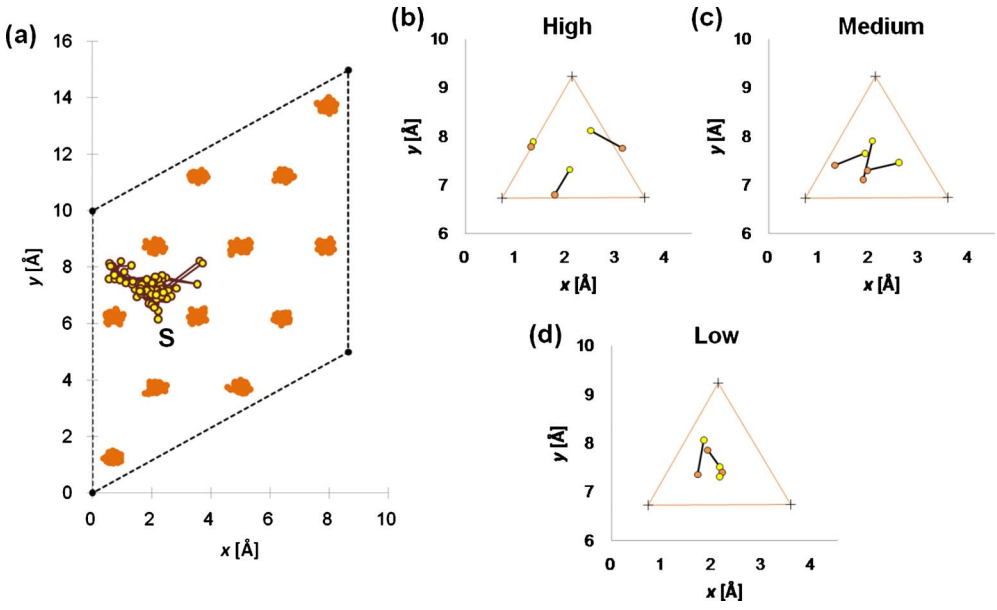

FIG. 2. (Color online) (a) Top views of the bottom S atom and the first surface-layer Au atoms of the bottom electrode taken form the 50 ps MD trajectories sampled at the 0.5 ps time interval (100 snapshots) for the conductance calculation (see Fig. 3). The S atom hops from a hollow site to another hollow site of the Au(111) surface and visits bridge sites along the way. Its maximum displacement amounts to 3.21 Å while that of the first surface-layer Au atoms is only 0.67 Å. The *xy* projections of the S-S lines from the three representative MD snapshot structures corresponding to the (b) high, (c) medium, and (d) low conductance values [see Figs. 3(c) and 4], respectively.

13.904 Å, 9.325 Å, and 2.767 Å, respectively, while those at the maximum tilt angle (10.84°) configuration (configuration A) were 13.742 Å, 9.398 Å, and 2.839 Å, respectively. On the other hand, at another configuration with a similarly large tilt angle of 10.52° (configuration B), we found the corresponding distances to be 13.997, 9.626, and 2.863 Å. That is, the large C6DT tilting accompanies the stretching of the S-Au bond distances plus a large fluctuation of the Au surface atoms (configuration A) or the stretching of the C6DT molecule (configuration B).

We next discuss the reliability of using FF to perform MD simulations, which is probably the biggest source of inaccuracy in our multiscale simulation approach. The most notable feature of our FF that was developed to describe Au organics and Au-Au interactions[26,27] was the adaptation of the nonbonded exponential-six-type function to describe the Au-organics interactions, which allows the S atom to hop from one site to another. In addition, our S-Au force parameters were constructed to reproduce the relative stability of an ethanthiolate (SCH_2CH_3) located on the ontop, fcc-hollow, and hcp-hollow sites of the (111) surface of a Au_{32} cluster calculated within the Becke-3-Lee-Yang-Parr (B3LYP) (Ref. 29) DFT level.[27] Together, these characters allow our FF to realistically model the true dynamics of organthiols on the Au surface, as demonstrated in a detailed study by Dirama and Johnson.[33] Although they have coupled our Au-Au and Au-organics force parameters with the AMBER FF (instead of the dreiding FF we intended), we expect that the overall conclusions will be similar. We further checked the reliability of our FF within our simulations by comparing the fluctuations of the FF potential energies with the DFT total energies calculated for the same MD snapshot geometries as shown in Fig. 3(b). The linear regression analysis of the fluctuations in the two energies summarized in Fig. 3(d) and the corresponding histograms shown in Fig. 3(e) indicate that our FF slightly underestimate the DFT energy fluctuations. However, it should be noted that our FF parameters were derived from B3LYP DFT calculations and the perfect correlation cannot be expected in Fig. 3(d). The R^2 value of 0.56 is rather small due to the several noticeable outliers but the closeness of the overall trends of the two data sets gives us additional confidence in the reliability of the sampled phase space within our FF.

We finally consider the statistical nature of the junction conductance arising from thermal fluctuations. Figure 3(c) shows the conductance fluctuation with time and Fig. 4(a) shows the corresponding development of a conductance histogram with the accumulation of data in the normal scale (bin size: $\Delta G = 10^{-3} G_0$). As emphasized in Sec. III A, due to the very large HOMO-LUMO energy gaps, conductance fluctuations should mainly result from the structural fluctuations of S-Au contacts. This is in contrast to the situation that involves conjugated molecules, for which overlaps between π-orbital molecular cores and Au 6*s* orbitals might play a more important role in determining the conductance.[15] Inspecting the contact geometries in more detail, although we could not extract any correlation between the Au-S or Au-Au distances and the conductance magnitude [Figs. 3(a) and 3(c)], we could determine that the S binding sites mainly determine the conductance variations. The contact geometries in which the S atoms bonded preferentially on the bridge [Figs. 2(b)] and hollow sites [Fig. 2(d)] of the bottom and top Au(111) surfaces result in the higher and lower conductance values, respectively, while the mixtures of the two result in the medium conductance values [Fig. 2(c)]. Because the zero-temperature energy-minimized structures of alkanedihiolates are based on the S binding to the fcc-hollow sites, the contact geometries that correspond to the lower end of the conductance distribution, we naturally obtain positively skewed histograms. Thus, we perform the Gaussian fitting to the conductance data shown on a logarithmic scale, and obtain the peak conductance $G = 0.0114 G_0$. The normalized log-G histograms [bin size: $\Delta \log(G/G_0) = 0.1$] presented in Figs. 3(b)–3(d) for the 100, 200, and 300 data points, respectively, reveal that 100 data points are already enough to provide us with a quite converged histogram. Con-

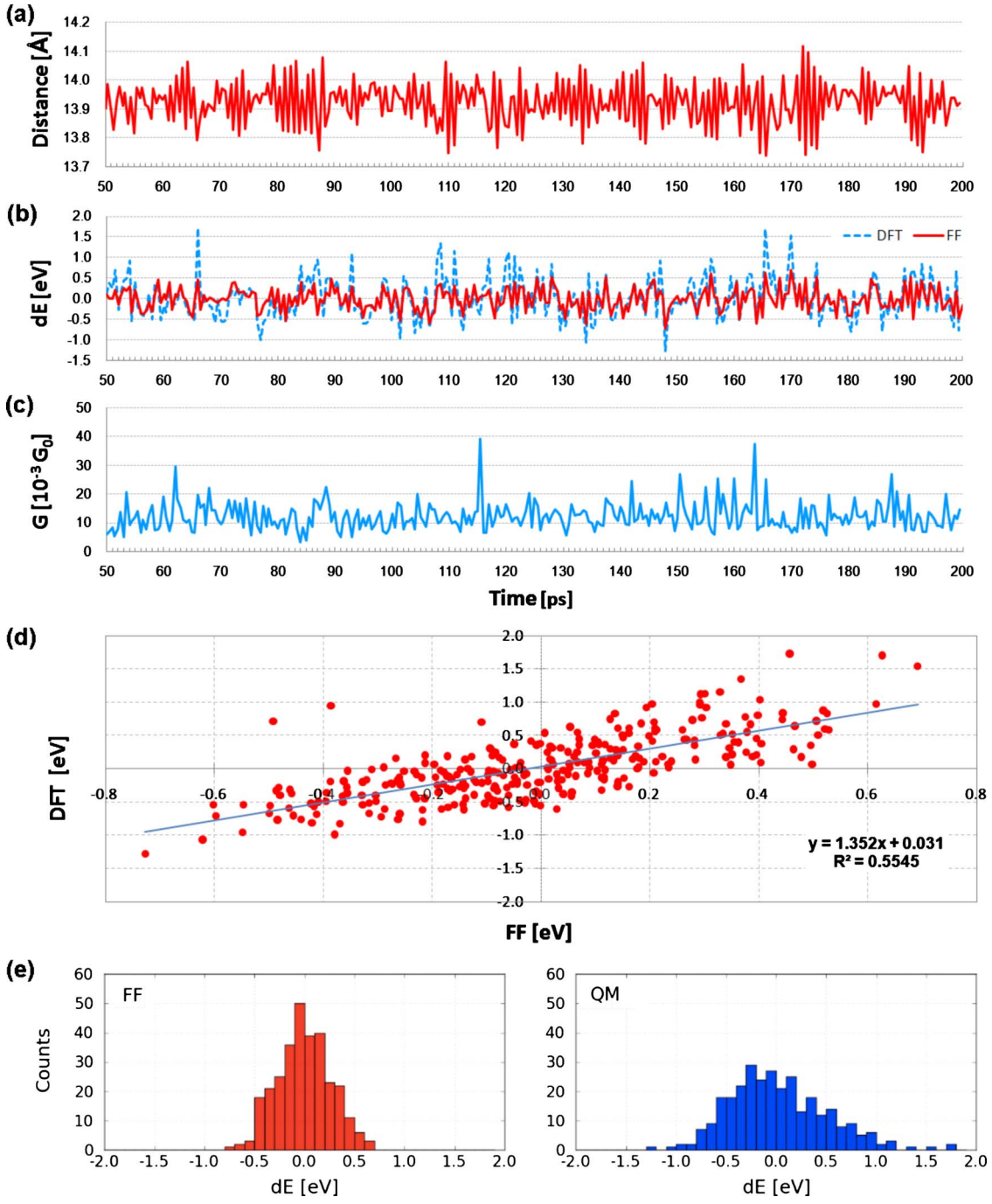

FIG. 3. (Color online) The fluctuations of the (a) Au-Au electrode distance, (b) FF potential and DFT total energies relative to their average values, and (c) conductance versus MD simulation time. (d) The correlation between the FF potential energies and DFT total energies calculated for the sampled 300 MD snapshot geometries, and (e) their histograms.

sidering the complexity of experimental situations and the resulting large number of data samples required,[5] this clearly demonstrates the advantage of computer simulations.

We close this section by providing two additional discussions. First because we observed a single conductance peak irrespective of the mobility of S atoms [Fig. 2(a)], we conclude that the involvement of different binding sites within the present S-Au contact model based on the direct coupling (not involving Au adatoms or wires) of the S atoms to the flat Au(111) surfaces cannot explain the current controversies on the multiple conductance peaks.[1,3,7–11] However, the appearance of a single well-defined conductance peak within the present molecule-metal contact model lays the foundation for our future study of more realistic junction models. Next, we observe that the average conductance of the thermally fluctuating C6DT, $G=0.0114G_0$, is 26% larger than that from the geometry optimized within FF, $G=0.0091G_0$.[24] This results in an increased difference from the experimental results (the maximum of the reported multiple conductance peak values is $2.6\times10^{-3}G_0$), which probably results from the underesti-

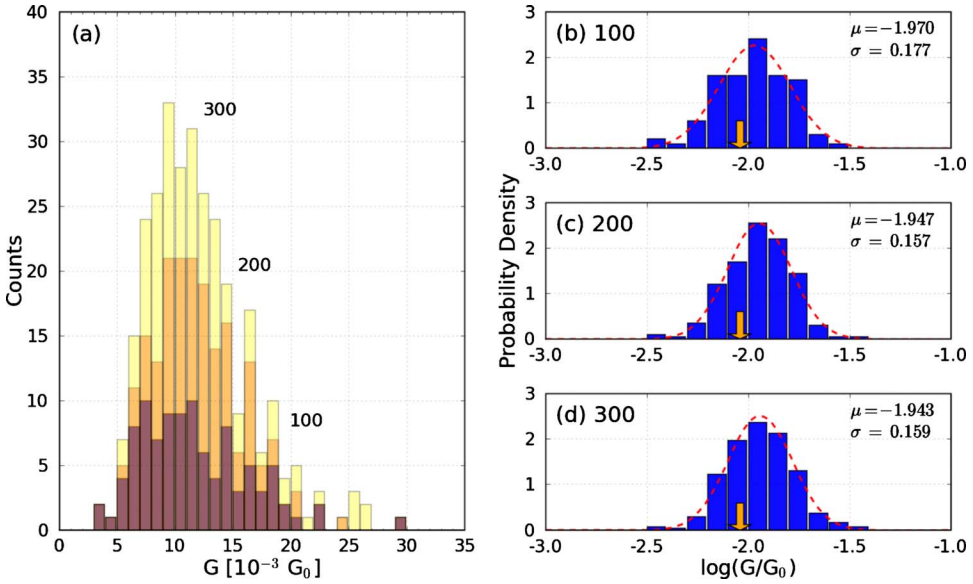

FIG. 4. (Color online) (a) The buildup of the conductance histogram from the 100, 200, and 300 MD snapshots (sampled at the 0.5 ps intervals) shown on the normal scale. The conductance histograms of the (b) 100, (c) 200, and (d) 300 MD snapshots shown on the logarithmic scale and their Gaussian fits. The arrow indicates the G value calculated for the zero-temperature FF-optimized geometry.

mation of the HOMO-LUMO gaps within GGA.[23] Irrespective of the GGA-resulting deficiency, however, we can point out a possible source of errors in comparing experimental conductance data obtained at a finite temperature and the theoretical data typically obtained for the zero-temperature energy-minimized structures.

IV. CONCLUSIONS

The alkanedithiolate molecules stretched between Au electrodes are ideal systems to study the charge transport across molecule-electrode contacts because the alkane molecular cores have large HOMO-LUMO gaps and only act as a simple tunneling barrier. In spite of their straightforward nature and much progress made in the MBJ techniques, there remain important discrepancies on the measured conductance values and their scaling behavior. Theory based on first-principles calculations can potentially resolve the problem but most previous calculations were based on static molecular geometries and the role of the important thermal fluctuations, especially those of the molecule-metal contacts, has been so far rarely discussed.[15,16] In this work, we automated our multiscale computational approach that combines classical FF MD simulations and quantum-mechanical DFT and MGF calculations, and, in particular, carefully checked the reliability of our FF in describing the mobile S-Au contact structures. Next, applying the updated method to an ideal junction model, we found that the direct S atom binding to the flat Au(111) surfaces produces a single conductance peak irrespective of the mobile nature of the S atoms, which jump from a hollow site to another hollow site and visit the bridge sites on the way. So, the important unresolved issue in experiments on the multiple conductance peaks could not be explained by the involvement of different Au surface sites within the considered ideal S-Au contact model.[1,3,7–11] However, at the same time, we confirmed that it can be used as a well-defined reference contact model for the future studies of more realistic junction geometries. Finally, we found that the optimized geometries in which the S atoms sit at the hollow sites correspond to the low-value side of conductance histograms. This resulted in a positively skewed conductance distribution, which can be better fit on a logarithmic scale, and a higher MD-derived conductance value compared with that from optimized geometries.

ACKNOWLEDGMENT

This work was supported by the University of Seoul 2009 Academic Research Fund.

*Corresponding author; y.h.kim@uos.ac.kr

[1] F. Chen, J. Hihath, Z. Huang, X. Li, and N. J. Tao, Annu. Rev. Phys. Chem. **58**, 535 (2007).
[2] H. B. Akkerman and B. de Boer, J. Phys.: Condens. Matter **20**, 013001 (2008).
[3] B. Xu and N. J. Tao, Science **301**, 1221 (2003).
[4] L. Venkataraman, J. E. Klare, I. W. Tam, C. Nuckolls, M. S. Hybertsen, and M. L. Steigerwald, Nano Lett. **6**, 458 (2006).
[5] M. T. González, S. Wu, R. Huber, S. J. d. Molen, C. Schönenberger, and M. Calame, Nano Lett. **6**, 2238 (2006).
[6] S.-Y. Jang, P. Reddy, A. Majumdar, and R. A. Segalman, Nano Lett. **6**, 2362 (2006).
[7] X. Li, J. He, J. Hihath, B. Xu, S. M. Lindsay, and N. J. Tao, J. Am. Chem. Soc. **128**, 2135 (2006).
[8] A. Nishikawa, J. Tobita, Y. Kato, S. Fujii, M. Suzuki, and M. Fujihira, Nanotechnology **18**, 424005 (2007).
[9] C. Li, I. Pobelov, T. Wandlowski, A. Bagrets, A. Arnold, and F. Evers, J. Am. Chem. Soc. **130**, 318 (2008).
[10] M. T. González, J. Brunner, R. Huber, S. Wu, C. Schönenberger, and M. Calame, New J. Phys. **10**, 065018 (2008).

[11] J. Zhou, F. Chen, and B. Xu, J. Am. Chem. Soc. **131**, 10439 (2009).
[12] Y. Hu, Y. Zhu, H. Gao, and H. Guo, Phys. Rev. Lett. **95**, 156803 (2005).
[13] K.-H. Müller, Phys. Rev. B **73**, 045403 (2006).
[14] S. Y. Quek, L. Venkataraman, H. J. Choi, S. G. Louie, M. S. Hybertsen, and J. B. Neaton, Nano Lett. **7**, 3477 (2007).
[15] D. Q. Andrews, R. P. Van Duyne, and M. A. Ratner, Nano Lett. **8**, 1120 (2008).
[16] M. Paulsson, C. Krag, T. Frederiksen, and M. Brandbyge, Nano Lett. **9**, 117 (2009).
[17] H. Cao, J. Jiang, J. Ma, and Y. Luo, J. Am. Chem. Soc. **130**, 6674 (2008).
[18] R. Maul and W. Wenzel, Phys. Rev. B **80**, 045424 (2009).
[19] Y.-H. Kim, S. S. Jang, Y. H. Jang, and W. A. Goddard III, Phys. Rev. Lett. **94**, 156801 (2005).
[20] Y.-H. Kim, S. S. Jang, and W. A. Goddard III, Appl. Phys. Lett. **88**, 163112 (2006).
[21] Y.-H. Kim and W. A. Goddard III, J. Phys. Chem. C **111**, 4831 (2007).
[22] Y.-H. Kim, J. Nanosci. Nanotechnol. **8**, 4593 (2008).
[23] Y.-H. Kim, J. Tahir-Kheli, P. A. Schultz, and W. A. Goddard III, Phys. Rev. B **73**, 235419 (2006).
[24] Y.-H. Kim, J. Korean Phys. Soc. **52**, 1181 (2008).
[25] C. George, H. Yoshida, W. A. Goddard III, S. S. Jang, and Y.-H. Kim, J. Phys. Chem. B **112**, 14888 (2008).
[26] Y.-H. Kim, S. S. Jang, and W. A. Goddard III, J. Chem. Phys. **122**, 244703 (2005).
[27] S. S. Jang, Y. H. Jang, Y.-H. Kim, W. A. Goddard III, A. H. Flood, B. W. Laursen, H.-R. Tseng, J. F. Stoddart, J. O. Jeppesen, J. W. Choi, D. W. Steuerman, E. DeIonno, and J. R. Heath, J. Am. Chem. Soc. **127**, 1563 (2005).
[28] J. P. Perdew, K. Burke, and M. Ernzerhof, Phys. Rev. Lett. **77**, 3865 (1996).
[29] M. Fuchs and M. Scheffler, Comput. Phys. Commun. **119**, 67 (1999).
[30] H. P. Langtangen, *Python Scripting for Computational Science*, 3rd ed. (Springer-Verlag, Berlin, 2008).
[31] M. Di Ventra, *Electrical Transport in Nanoscale Systems* (Cambridge University Press, Cambridge, 2008).
[32] G. K. Ramachandran, T. J. Hopson, A. M. Rawlett, L. A. Nagahara, A. Primak, and S. M. Lindsay, Science **300**, 1413 (2003).
[33] T. E. Dirama and J. A. Johnson, Langmuir **23**, 12208 (2007).